International Journal of Precision Engineering and Manufacturing (2019) 20:217–232
https://doi.org/10.1007/s12541-019-00031-1

Online ISSN 2005-4602
Print ISSN 2234-7593

REGULAR PAPER

Springback Analysis of the Stiffened Panel Milling from the Bent Plate

Chun-Guo Liu[1,2] · Tao Yue[1,2] · Xiao-Tong Yu[1,2]

Received: 20 August 2018 / Revised: 2 January 2019 / Accepted: 23 January 2019 / Published online: 14 February 2019

Abstract

An analytical method considering the redistribution of residual stress in the bent plate is proposed to predict the springback of the stiffened panel when milling the panel layer by layer. Two types of stiffened panel, namely, a panel with crosswise stiffeners and a panel with lengthwise stiffeners, were selected as examples and were analyzed during the removal of each layer. Moreover, a finite-element simulation of the milling process was conducted to make comparisons with the analytical results, which demonstrates similar stress distribution and springback values. The maximum stress variation and springback value appeared when the milling depth reached the initial neutral surface. When the plate thickness decreased, the errors between analytical results and FEM results increased, and the lengthwise-stiffened panel was less affected by errors than the crosswise-stiffened panel because of a larger moment of inertia. The effects of different milling thicknesses per layer, initial plate thickness, and bending radius were also analyzed. Moreover, the milling experiment was performed to make verification. The results suggest that the analytical method can predict the springback of the stiffened panel effectively. The proposed method can also be applied to other similar forming conditions.

Keywords Residual stress · Springback · Milling · Bent plate · FE simulation

List of symbols

t	Half of the plate thickness
Δt	The thickness of removed layer
t_1, t_2	The thickness of the stiffer and the plate
h	The height of the stiffener
Z_c	The centroid of the cross section
E	The elastic modulus
σ_x	The stress in x-direction
σ_s^*	The principal stress
σ_s	The initial yield stress
σ_x'	The residual stress in the lengthwise stiffeners
ε	The strain
ε_e	The strain caused by milling after springback
m	Hardening index
A	Hardening coefficient
μ	Poisson ratio
b	The width of the plate
κ	The curvature of the plate
n	The times of milling
y_s	Distance between initial yield surface and the neutral surface
M	The bending moment
M_{bend}	The bending moment in the bending process
M_e	The bending moment when the surface of the plate starts to yield
$\Phi(\kappa)$	The function of the bending moment and the curvature
κ_f	The curvature after springback
α, α'	The bending angle of the plate before and after springback,
y, y'	The y coordinate before and after springback
$\Delta L, \Delta L'$	The elongation of the y-th layer before and after springback
r, r'	The radius of the neutral surface before and after springback
I	The moment of inertia
I_1, I_2	The moment of inertia of the stiffer and the plates

✉ Chun-Guo Liu
liucg@jlu.edu.cn; liucg@jlu.edu.cn

Tao Yue
435954155@qq.com

Xiao-Tong Yu
1210432310@qq.com

[1] Roll Forging Research Institute, Jilin University (Nanling Campus), Changchun 130025, People's Republic of China

[2] College of Materials Science and Engineering, Jilin University (Nanling Campus), Changchun 130025, People's Republic of China

I_z	The moment of inertia of the plate after milling
η	The springback ratio
λ	The ratio of y_s and t
σ_{res}	The residual stress after springback
σ_{res}^1	The stress after the first layer is milled
σ_{res}^n	The stress after the n-th layer is milled
σ_{res}^s	The residual stress in the plate of the stiffened panels after springback
F_m	The stress released after milling
M_m	The bending moment released after millng
$F_{\mathrm{m}}^{\mathrm{n}}$, $M_{\mathrm{m}}^{\mathrm{n}}$	The stress and the bending moment caused by the removal of the n-th layer
F_{fin}, M_{fin}	The total stress and bending moment caused by milling process
k_1, k_2	The coefficients of the stress increment increment for the upper and lower sides
k_1^n, k_2^n	The coefficients of linear stress increments after the n-th layer is milled

1 Introduction

Springback is a critical issue in the aviation manufacturing industry, particularly for the production of stiffened panels [1, 2]. Generally, in the manufacturing process of these panels, a plate will be milled into a stiffened panel and formed into the desired shape by rolling, press bending, peen forming, or creep forming. For panels with large deformation, rolling and press bending are the most efficient processing methods. However, in the bending process, since the stiffeners may be damaged and cannot fulfill the high quality requirements [3, 4], an alternative manufacturing process for stiffened panels has been proposed. In this process, the plate is first bent or rolled to the desired shape, clamped onto the fixture and milled into the final stiffened panel using a high-speed milling machine. During the milling process, the residual stress release generates a bending moment and a bending force on the plate, which redistributes the residual stress in the remaining plate. However, this process requires a large clamp force, and the workpiece should be positioned on the fixture. Furthermore, the springback of the panel after unloading also affects the final accuracy. Hence, a study of the residual stress relaxation during the milling process and springback of the workpiece is of great value.

Many studies have investigated the relationship between the residual stress and the milling process. Meng [5] presented a new model to measure the equivalent residual stress and depth of the affected layers generated by milling using the strain change on the opposite side of each removed layer. Krottenthaler [6] focused on the ion beam milling and digital image correlation to measure the residual stress in thin films by removing materials to form an H-bar geometry. Sebastiani [7] also evaluated the residual stress and Poisson's ratio using a novel method based on a two-step, four-slot micro-milling process and validated this method through modeling and experiments; however, the methodology was only suitable for small material volumes. Vilček [8] evaluated the generation of the residual stress in precision milling using a deflection-electrochemical etching technique and obtained the residual stress distribution through the milling process.

The milling process also generates a machine-induced residual stress with a high magnitude, which significantly affects the surface integrity [9–11]. The machining parameters, material characteristics and tool geometry should be considered. Sun [12] performed a series of end-milling experiments and revealed that the compressive residual stress in the feed direction increased with the cutting speed and magnitude. The distribution of residual stress was determined from a highly nonlinear coupling of mechanical and thermal loadings. The maximum machined-surface residual stress (MMSRS) was 400 MPa, and the depth of machined residual stress (DMRS) was less than 50 μm. Arunachalam [13] investigated the differences in residual stress caused by the cubic boron nitride and ceramic cutting tools under various cutting conditions such as speed, depth of cut, and tool geometry. The results showed that the MMSRS was 1200 MPa for different cutting tool materials. Li [14] measured the residual stress in different zones of thin-walled parts as a function of the depth of cut, where the MMSRS was approximately 200 MPa, and the DMRS was 60–90 μm. Ma [15] analyzed the relationship between the cutting force and the temperature loading with residual stress and found that the MMSRS was approximately 300 MPa. Although the aforementioned studies suggest that the milling process will generate significant residual stress, the depth of cut does not exceed 200 μm, which has minimal effect on the stress redistribution of the entire component. In this work, the additional residual stress caused by the milling process was neglected when the springback and stress distribution were analyzed.

The analytical method reveals the physical principle of the residual stress variation during the machining process, but it is also the most difficult method to analyze the residual stress because many assumptions are required to simplify complex issues. Liang [16] established a predictive model for residual stress using process conditions as the inputs, such as the cutting forces and cutting temperatures. Similarly, Huang [17] proposed an analytical approach to obtain the residual stress at different depths of a machined surface.

The finite-element method (FEM) offers an effective approach to investigate the residual stress distribution because it can provide much detailed information without complicated experiments. As an example, Salahshoor [18] used the FEM to predict the process-induced residual stress in high-speed dry milling and validated the method via experiments. Yang [19] combined the FEM and a statistical model to analyze the residual stress in peripheral milling to improve its efficiency. Hua [20] implemented the hardness-based flow stress model encapsulated in an FE program to study the residual stress distribution in a machined surface and the effects of cutting conditions and tool geometry. With further development of the FE software, numerical simulations may offer more reliable results.

In this paper, an analytical method is proposed to predict the springback of a stiffened panel, which was milled from a cylindrical bent thick plate. The proposed method considers the redistribution of residual stress in the remaining plate after milling. Two types of stiffened panels were selected as objects of study, which had crosswise and lengthwise stiffeners, respectively. An FEM analysis was conducted to make comparisons with the analytical results. Moreover, the effect of different milling thicknesses per layer, initial plate thickness, and bending radius were analyzed. The milling experiment was also performed to make verification. The proposed method can also be applied to other similar forming conditions.

2 Residual Stress Analyses During Layer-by-Layer Milling

2.1 Residual Stress After Bending

The coordinate system was established as shown in Fig. 1, where the original point was set on the middle surface of the plate. A uniform distribution of the residual stress of each layer along the length of the plate was assumed. The thickness of the plate was $2t$, and the neutral surface was assumed to be always in the center of the plate.

By Hooke's law and Hollomon's law, when the plate was cylindrical bent, the stress in x-axis along thickness was:

$$\sigma_x = \begin{cases} E\varepsilon, & \varepsilon \le \sigma_s/E \\ \sigma_s + A\left(\varepsilon - \frac{\sigma_s}{E}\right)^m, & \varepsilon \ge \sigma_s/E \end{cases} \tag{1}$$

where σ_s is the initial yield stress, E is the elastic modulus, ε is the strain in x-direction, m and A refer to the hardening index and hardening coefficient, respectively.

According to Mises yield condition, the principal stresses are expressed as:

$$\sigma_s^* = \sigma_x = \frac{\sigma_s}{\sqrt{1 - \mu + \mu^2}} \tag{2}$$

And the bending moment to the neutral surface can be expressed as follows [21]:

$$\begin{aligned} M_{bend} &= 2\int_0^{y_s} \sigma_x b y dy + 2\int_{y_s}^{t} \left[\sigma_s^* + A\left(\varepsilon - \frac{\sigma_s^*}{E}\right)^m\right] b y dy \\ &= \sigma_s^* b t^2 - \frac{\sigma_s^{*3} b}{3E^2\kappa^2} + A\left(\varepsilon - \frac{\sigma_s^*}{E}\right)^m b(t^2 - y_s^2) \end{aligned} \tag{3}$$

where b is the width of the plate; κ is the curvature of the plate, and y_s is where is the distance between initial yield surface and the neutral surface. When the surface of the plate starts to yield, the bending moment can be obtained:

$$M_e = 2E\kappa \int_0^t b y^2 dy = \frac{2}{3}\sigma_s^* b t^2 \tag{4}$$

Then the function of bending moment and curvature can be expressed as:

$$\Phi(\kappa) = M \tag{5}$$

When the plate is unloaded, the springback process is equivalent to the elastic deformation caused by a reverse bending moment M', whose value is $-M$. Thus the curvature after springback can be derived as:

$$\kappa_f = \Phi^{-1}(M) - \frac{M}{EI} \tag{6}$$

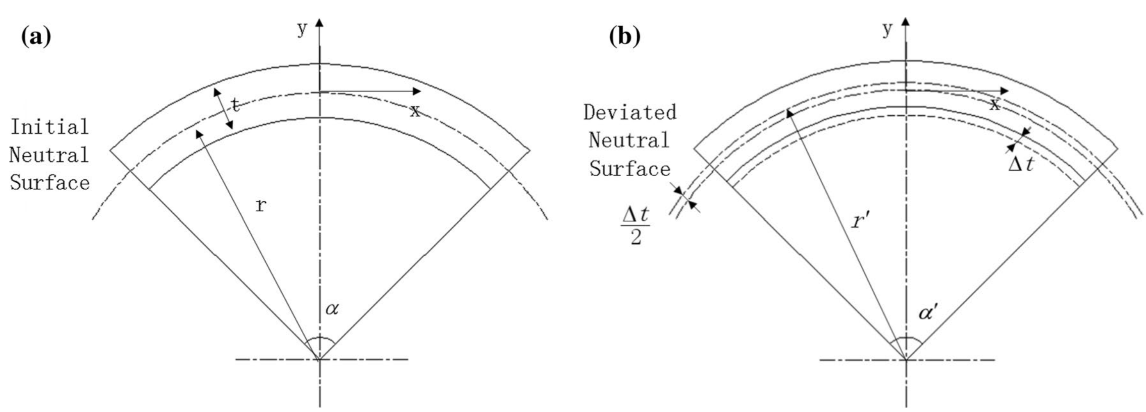

Fig. 1 Schematic figure of the plate after bending

where I is the moment of inertia of the plate. Based on Eqs. (2)–(6), the springback ratio can be express as:

$$\eta = \frac{\kappa_f}{\kappa} = \frac{\Phi^{-1}(M) - M/EI}{\Phi^{-1}(M)} = 1 - \frac{2y_s M}{tM_e} = \left[1 - \frac{3}{2}\lambda + \frac{1}{2}\lambda^3 - \frac{3A\sigma_s^{*m-1}(1-\lambda)^{m+1}(m+\lambda+1)}{E^m\lambda^{m-1}(m+1)(m+2)}\right]^{-1} \quad (7)$$

where λ is equal to y_s/t.

Moreover, the residual stress can be derived as:

$$\sigma_{res} = \begin{cases} Ey\kappa_f, & (-y_s \le y \le y_s) \\ Ey(\kappa_f - \kappa) + A(y\kappa - \sigma_s^*/E)^m, & (y_s \le y \le t/2) \\ Ey(\kappa_f - \kappa) + A(y\kappa + \sigma_s^*/E)^m, & (-y_s \le y \le -t/2) \end{cases} \quad (8)$$

$$\begin{cases} F_m = \int_{\Delta t/2}^{t/2} \left[\sigma_{res} + k_1(y - \Delta t/2)\right] bdy + \int_{-t/2+\Delta t}^{\Delta t/2} \left[\sigma_{res} + k_2(y - \Delta t/2)\right] bdy \\ M_m = \int_{\Delta t/2}^{t/2} \left[\sigma_{res} + k_1(y - \Delta t/2)\right](y - \Delta t/2) bdy + \int_{-t/2+\Delta t}^{\Delta t/2} \left[\sigma_{res} + k_2(y - \Delta t/2)\right](y - \Delta t/2) bdy \end{cases} \quad (11)$$

2.2 Residual Stress Redistribution During Milling Process

The difference in derivation process between milling from concave and convex surfaces was the coordinate of the neutral surface after the deviation. Here, the case of milling from a concave surface is presented as an example.

When the first layer was removed, the residual stress was released, which would apply a reverse bending moment and force on the remaining plate. Assuming that the thickness of the removed layer is Δt, the moment and force are expressed as:

$$\begin{cases} F_m = \int_{-t/2}^{-t/2+\Delta t} \sigma_{res} dy \\ M_m = \int_{-t/2}^{-t/2+\Delta t} \sigma_{res} y dy \end{cases} \quad (9)$$

Since the neutral surface is in the middle surface of the plate, it will move upwards by $\frac{\Delta t}{2}$, as shown in Fig. 1b. The residual stress distribution in the remaining plate satisfies the following conditions:

$$\begin{cases} -F_m = \int_{-t/2}^{-(t/2-\Delta t)} \sigma_{res} bdz \\ -M_m = \int_{-t/2}^{-(t/2-\Delta t)} \sigma_{res} ybdz \end{cases} \quad (10)$$

After the first layer is removed, the stress increment and bending moment increment are $-F_m$ and $-M_m$, respectively. It is supposed that the stress increments on the both sides of the deviated neutral surface are linearly distributed, and the slopes for the upper and lower sides are k_1 and k_2, respectively. Then the following equations can be derived:

Then, the formulas can be solved as:

$$k_1 = k_2 = \frac{-F_m \Delta t}{16 I_z} \quad (12)$$

where I_z is the moment of inertia of the plate after milling. Then, the stress redistribution after the first layer is milled is expressed as:

$$\sigma_{res}^1 = \begin{cases} \sigma_{res} + k_1(y - \Delta t/2), \Delta t/2 < y < t/2 \\ \sigma_{res} + k_2(y - \Delta t/2), -(t - 2\Delta t)/2 < y < \Delta t/2 \end{cases} \quad (13)$$

When the n-th layer is milled, the residual stress release is expressed as:

$$\begin{cases} F_m^n = -\int_{-t/2+(n-1)\Delta t}^{-(t/2-n\Delta t)} \sigma_{res}^{n-1} bdz \\ M_m^n = -\int_{-t/2+(n-1)\Delta t}^{-(t/2-n\Delta t)} \sigma_{res}^{n-1} \left[y - \frac{(n-1)\Delta t}{2}\right] bdz \end{cases} \quad (14)$$

where F_m^n and M_m^n are the respective stress and bending moment load applied on the remaining plate caused by the removal of the n-th layer and satisfy the following equations:

$$\begin{cases} F_m^n = \int_{n\Delta t/2}^{t/2} \left[\sigma_{res}^{n-1} + k_1^n(y - n\Delta t/2)\right] bdy + \int_{-t/2+n\Delta t}^{n\Delta t/2} \left[\sigma_{res}^{n-1} + k_2^n(y - n\Delta t/2)\right] bdy \\ M_m^n = \int_{n\Delta t/2}^{t/2} \left[\sigma_{res}^{n-1} + k_1^n(y - n\Delta t/2)\right](y - n\Delta t/2) bdy + \int_{-t/2+n\Delta t}^{n\Delta t/2} \left[\sigma_{res}^{n-1} + k_2^n(y - n\Delta t/2)\right](y - n\Delta t/2) bdy \end{cases} \tag{15}$$

where k_1^n and k_2^n are the respective coefficients of linear stress increments after the n-th layer is milled, which can be solved as:

$$\begin{cases} k_1^n = \dfrac{\left[M_m^{n-1} - \Delta t/2(F_m^{n-1} - F_m^n)\right] - 2F_m^{n-1}(t/2 - n\Delta t)}{4I_z} \\ k_2^n = \dfrac{\left[M_m^{n-1} - \Delta t/2(F_m^{n-1} - F_m^n)\right] + 2F_m^{n-1}(t/2 - n\Delta t)}{4I_z} \end{cases} \tag{16}$$

Then, the stress of the remaining plate is obtained as follows:

$$\sigma_{res}^n = \begin{cases} \sigma_{res} + \sum_{i=1}^{n} k_1^n(y - n\Delta t/2), n\Delta t/2 < y < t/2 \\ \sigma_{res} + \sum_{i=1}^{n} k_2^n(y - n\Delta t/2), -(t - 2n\Delta t)/2 < y < n\Delta t/2 \end{cases} \tag{17}$$

The total stress and bending moment caused by milling process can be expressed as:

$$\begin{cases} M_{fin} = \sum_{i=1}^{n} M_m^i \\ F_{fin} = \sum_{i=1}^{n} F_m^n \end{cases} \tag{18}$$

2.3 Springback Calculation for Different Stiffened Panels

When the plate is unloaded, the external constraint disappears, and springback occurs. It is assumed that the radius of the neutral surface after springback is r', which can be derived as follows:

$$\Delta\kappa = \frac{bM_{fin}}{EI_z} = \frac{1}{r'} - \frac{1}{r + n\Delta t/2} \tag{19}$$

Here two types of stiffened panels are discussed, which have crosswise or lengthwise stiffeners (Fig. 2).

To calculate the moment of inertia of the cross section I_z, the middle plane of the plate of the stiffened panel was selected as the reference plane. Thus, for the panel in Fig. 2a, I_z is calculated as follows:

$$\begin{cases} I_1 = \frac{1}{12} t_1 h^3 + (h/2 + t_2/2 - Z_c)^2 t_1 h \\ I_2 = \frac{1}{12} t_2^3 b + Z_c^2 t_2 b \\ I_z = I_1 + I_2 \end{cases} \tag{20}$$

where t_1 is the thickness of the stiffener; t_2 is the thickness of the plate; I_1 is the moment of inertia of the stiffeners; I_2 is the moment of inertia of the plate; h is height of the stiffener; and Z_c is the distance from the centroid of the cross section of the stiffened panel to the reference plane, which is calculated as follows:

$$Z_c = \frac{t_1 h(h/2 + t_2/2)}{t_1 h + t_2 b} \tag{21}$$

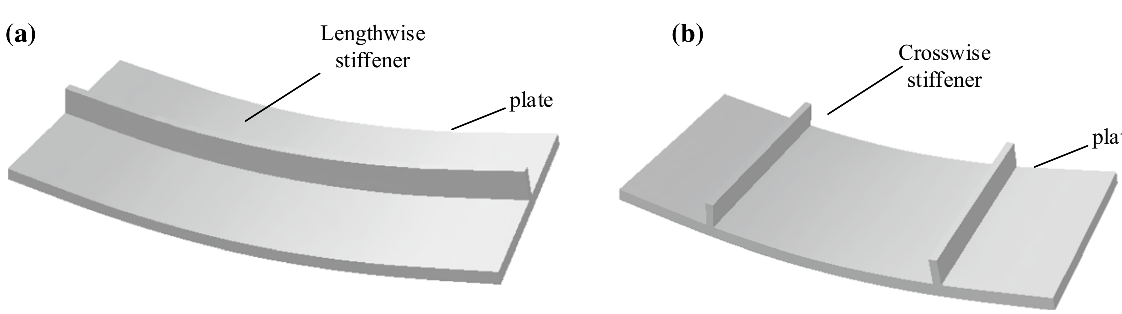

Fig. 2 Two types of stiffened panels

For the panel in Fig. 2b, I_z is expressed as:

$$I_z = \frac{t_2^3 b}{12} \tag{22}$$

Before springback, it is assumed that the length of the y-th layer after bending is:

$$\Delta L = (r + y)\alpha \tag{23}$$

which will change to the following formula after springback:

$$\Delta L = (r' + y' - \Delta t/2)\alpha \tag{24}$$

where α and α′ are the bending angle of the plate before and after springback, respectively, as presented in Fig. 1; and y' is equal to y. Then, the strain caused by milling after sptingback is derived as:

$$\varepsilon_e = \frac{\Delta L' - \Delta L}{\Delta L} = \frac{(r' + y' - \Delta t/2)\alpha - (r + y)\alpha}{(r + y)\alpha} \tag{25}$$

In the derivation, the following condition is also obtained because the strain in the neutral surface is 0:

$$(r + \Delta t/2)\alpha = r'\alpha' \tag{26}$$

Then, Eq. (25) is rewritten as:

$$\varepsilon_e = \frac{(2y - \Delta t)(2r - 2r' + \Delta t)}{4(r + y)r'} \tag{27}$$

In addition, the springback will release the stress load and bending moment load. Then, the residual stress in the plate of the stiffened panels after springback is expressed as:

$$\sigma^s_{res} = \sigma^n_{res} + E\varepsilon_e + \frac{(2y - n\Delta t)M_{fin} b}{2I_z} + \frac{F_{fin}}{t - n\Delta t} \tag{28}$$

Since no material removal occurs on the stiffener, the variation in the residual stress is only caused by the change in strain. Thus, the residual stress in the crosswise stiffeners remains unchanged, whereas the residual stress in the lengthwise stiffeners can be represented as:

$$\sigma'_x = \sigma_{res} - E\varepsilon_e \tag{29}$$

3 Finite-Element Analyses and Milling Experiments

3.1 Finite Element Model

To validate the analytical model, a finite-element analysis was conducted to analyze the residual stress distribution and springback. An AL 7B04-T7451 plate was selected as the research object. The material model character belongs to the elastoplastic behavior with isotropic hardening. According

Table 1 Material parameters

Yield stress (MPa)	Young's modulus (GPa)	Poisson's ratio	Hardening index m	Hardening coefficient A
475	69.3	0.3	0.13	879

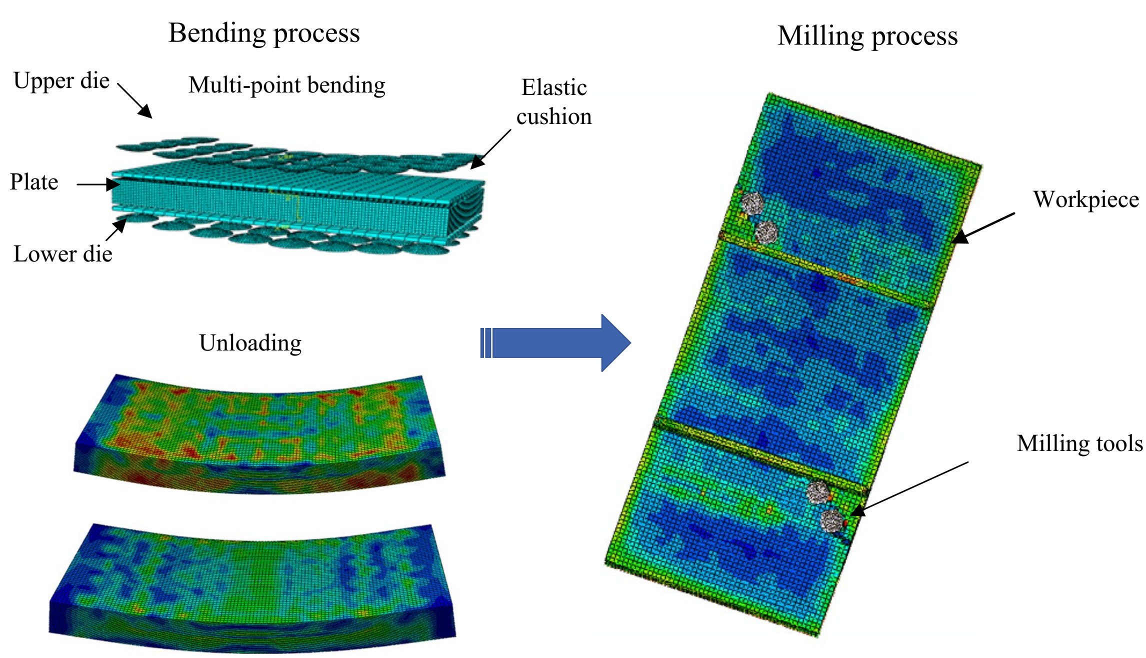

Fig. 3 Finite-element model of the process

Table 2 Simulation parameters

Friction coefficient	Fracture strain	Stress triaxia	Strain rate	Milling tool diameter (mm)
0.15	0.18	0.33	1	10

to the data of uniaxial tensile tests, it is expressed in exponential form. The mechanical properties of the material are listed in Table 1.

The simulation process including two procedures is shown in Fig. 3. Firstly, the plate was bent into designed radius. The Abaqus/Explicit was used for the procedure and the hardening type was selected as isotropic hardening in the simulation. The model consists of the multi-point die, the elastic cushion and the plate. The total element number is 72,263. The plate contained 55,000 elements, whose dimensions were 1 mm thick, 2 mm long and 2 mm wide. The element type of the plate and the cushion was C3D8R. To minimize the model, the die was simplified as a rigid shell of element type R3D4. In bending process, the lower die was fixed and the upper die moved down until the workpiece was in full contact with the lower die. The loading speed was 0.19 m/s, and the friction coefficient was set as 0.15. The unloading process was conducted with Abaqus/Standard. The bending simulation results were imported as the initial state and all restrains were removed. The central point was selected as the fixed point in order to make it springback spontaneously.

Table 3 Dimensions and the milling parameters of the stiffened panels

Variable	Parameters				Dimensions	
	Milling depth	Milling layer thickness	Plate thickness	Bending radius	Lengthwise	Crosswise
Milling depth	2, 4, 6, 8, 10, 12	2	20	600	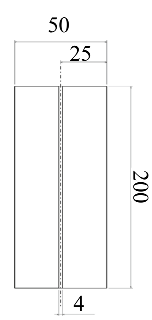	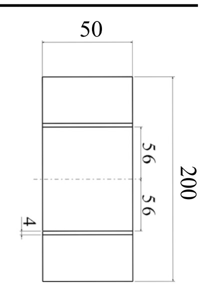
Milling layer thickness	12	1, 2, 3	20	600		
Plate thickness	12	2	18, 20, 22	600		
Bending radius	12	2	20	200, 400, 600		

For example, when the variable is "milling depth", in the corresponding row the variable value of the "milling depth" are "2, 4, 6, 8, 10, 12". The other parameters are constants: the "bending radius" is 600 mm, the "plate thickness" is 20 mm, and the "milling layer thickness" is 2 mm

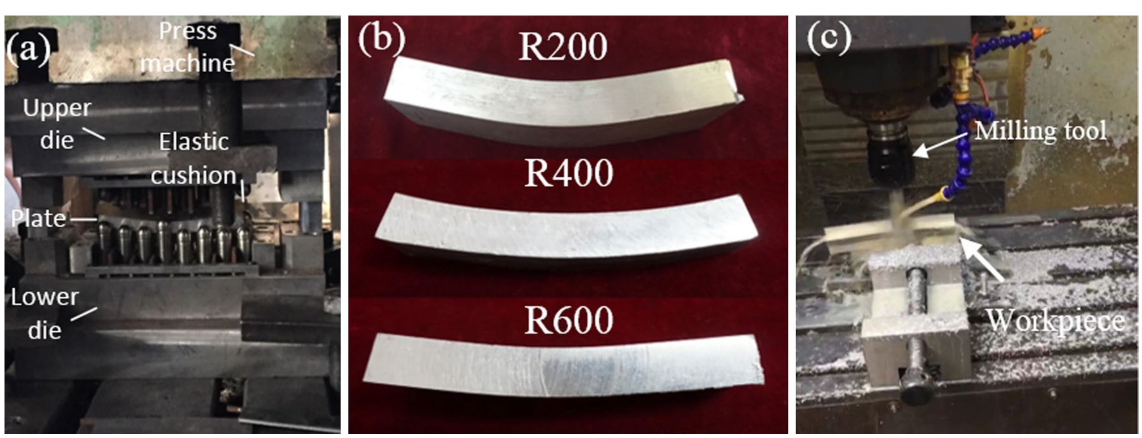

Fig. 4 Milling experiment. **a** Bending process, **b** bent plate and **c** milling process

The simulation of milling process was conducted with Abaqus/Explicit. In the process, the stress distribution status after springback was firstly imported into the model. Then the bottom of the plate was fixed, and the plate was milled into desired shape by controlling the path of milling tools. The diameter of the milling tools was 10 mm and the rotate speed was 10,000 rpm. The ductile damage model was used to calculate the failure of the material. The relevant parameters were obtained from material properties and were listed in Table 2. The interaction was surface-to-surface contact. After milling, the springback procedure was conducted again with Abaqus/Standard.

The milling process with two types of stiffened panels was simulated to make comparisons with the analytical values. The results at different milling depths were analyzed such as 2, 4, 6, 8, 10, and 12 mm, and each removed layer was 2 mm thick. Moreover, the milling process of different milling layer thicknesses, bending radii and plate thicknesses was simulated. The relevant dimensions, milling depth and milling layer thickness of each condition are shown in Table 3.

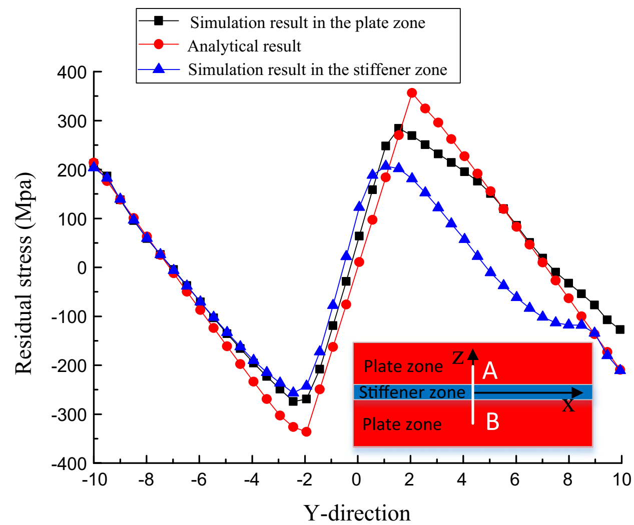

Fig. 6 Initial residual stress through thickness after bent for R400 mm

3.2 Milling Experiment

Twenty-millimeter-thick AL 7B04-T7451 plates were prepared for the experiment and cut into the dimensions of 200 mm × 50 mm. The plates were first bent into different bending radius (200, 400 and 600 mm) with multi-point forming process as shown in Fig. 4a. The die was regulated into desired shape, and positioned on the mold holder. The plate covered with elastic cushion was put on the lower die. The upper die was moved down until it was in full contact with the workpiece. After holding the pressure for a while, the die was moved away. Bending process was carried out on a hydraulic press whose capacity was 800 t. After the profile was measured, the bent plate was clamped and milled into stiffened panel with a 3-axis CNC milling machine.

Workpiece measurement was conducted by an NDI Procam 3000 three-dimensional laser scanner as shown in Fig. 5. During measurement, the three-dimensional coordinates of the workpiece were generated and uploaded to the Geomagic Qualify 2013 software. Then the profile data was required. Through the comparison with the profile data acquired from the analytical method, the errors of the two methods were obtained.

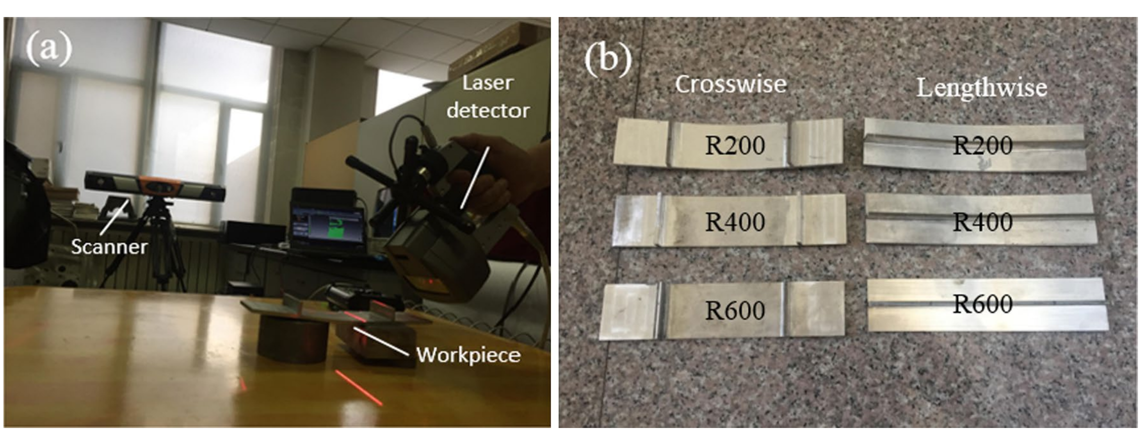

Fig. 5 The measurement of the workpiece. **a** The three-dimensional laser scanner and **b** the milled stiffened panel

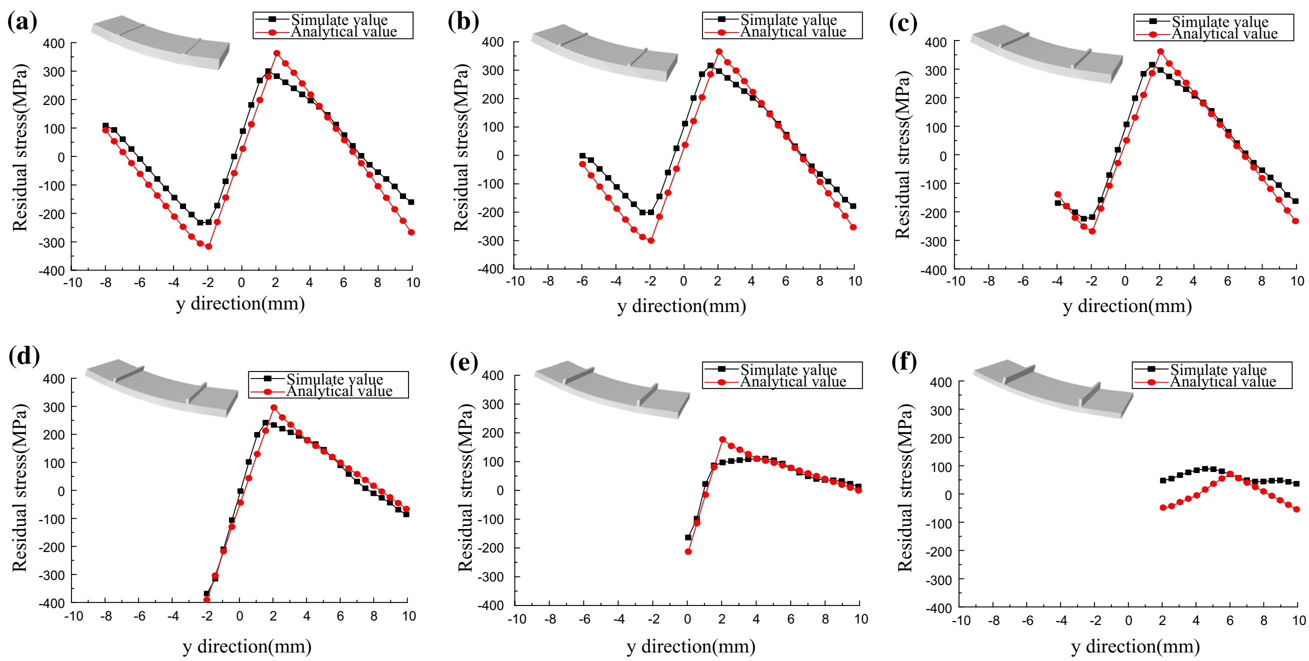

Fig. 7 Residual stress distribution of the crosswise-stiffened panel at cutting depths of **a–f** 2, 4, 6, 8, 10 and 12 mm

4 Result Analyses and Discussion

4.1 The Bending Residual Stress Distribution

Figure 6 shows the residual stress distribution in *x*-direction along the thickness when the bending radius was R400 mm. The comparisons of FEM value and analytical value were made to validate the formula (8). Since the target shape was symmetry, the central section (A–B) was selected as study region and the average residual stress distribution in plate area (the region will be milled away) and stiffener area (the region will be retained as stiffener) is obtained respectively. As shown in the figure, the simulation result of the residual stress in the plate matched well with the analytical result. The maximum error appeared in the elasto plastic interface and reached 74 MPa. The standard deviation of two curves was 41 MPa. However, for the result in the stiffener, there are greater differences in the stress distribution above the neutral layer. The main reason is the width of the stiffener is smaller and the data points are fewer, leading to larger error.

4.2 Residual Stress Distribution in Milling Process

The stress results in *x*-direction of the plate with the crosswise-stiffened panel are presented in Fig. 7. The residual stress distribution curves of two methods have identical variation trends and similar stress values. Compared with Fig. 6, when the plate was milled to 2 mm, the stress increased from -8 mm to 1 mm in the y-direction and decreased from 1 to 10 mm. However, when the milling depth changed from 6 to 10 mm, the stress decreased, which is consistent with the results of the analytical method. According to Eq. (10), when the milling depth is within 4 mm, the residual stress released is positive, and the distance to the neutral surface is negative, which makes the bending moment M negative and additional force F positive. Using formula (28), the residual stress on both sides of the neutral surface can be obtained, and the residual stress increases below the neutral surface and decreases above the neutral surface. When it is milled from 6 to 10 mm, the residual stress becomes negative, which makes the bending moment change sign and reversely increase. In this situation, the stress on both sides of the neutral surface increases in the opposite direction. The maximum stress variation reached 200 MPa at a milling depth of 10 mm, as shown in Fig. 7f. Equation (18) and Fig. 6 show that the bending moment varies with the increase in milling depth and maximizes at a depth of 10 mm. In Fig. 7f, the standard deviation of the two methods was 67 MPa, whereas the minimum error was 27 MPa in Fig. 7e.

The residual stress distributions *x*-direction in the plate with the lengthwise-stiffened panel are shown in Fig. 8, which are similar to the distributions in the panel with the crosswise stiffener. Figure 8d, e reveal that the maximum values of the stress and stress variation appeared at milling depths of 8 and 10 mm, respectively. The maximum standard deviation between the two curves was 55 MPa, as shown

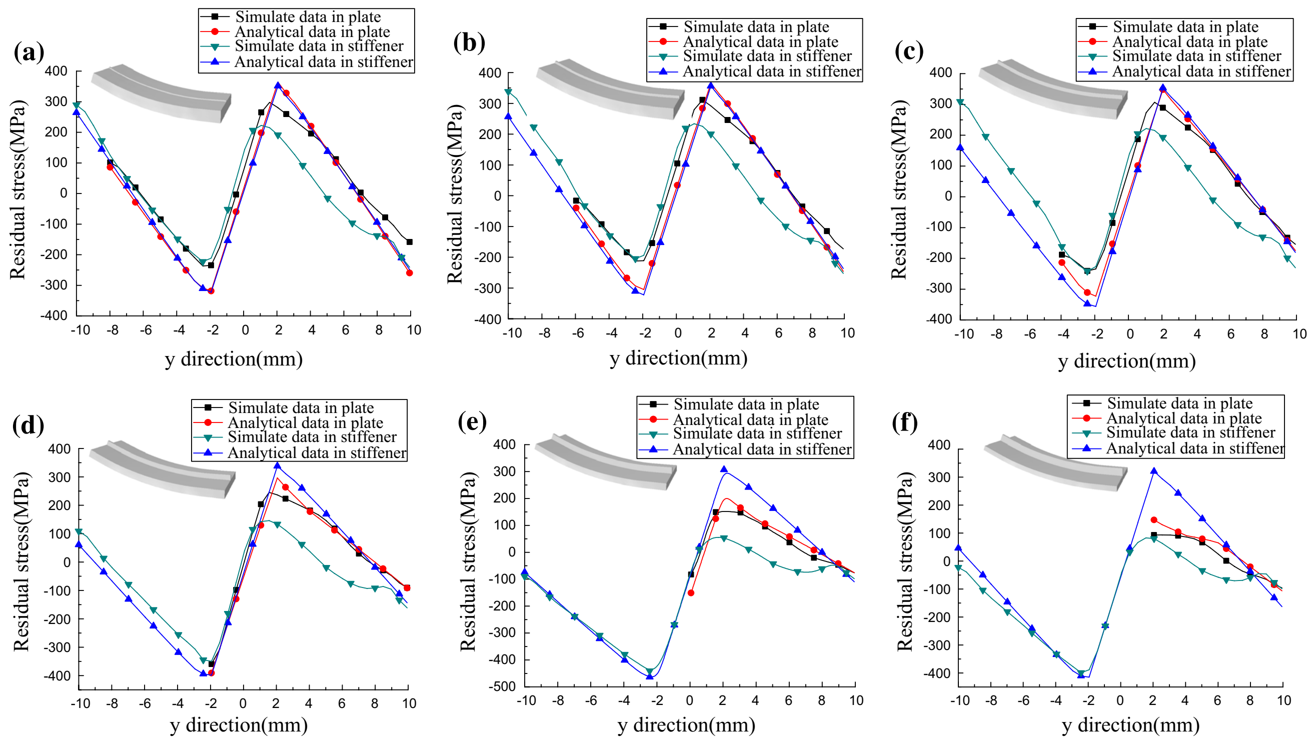

Fig. 8 Residual stress distribution of the lengthwise-stiffened panels: **a**–**f** cutting depth of 2, 4, 6, 8, 10 and 12 mm

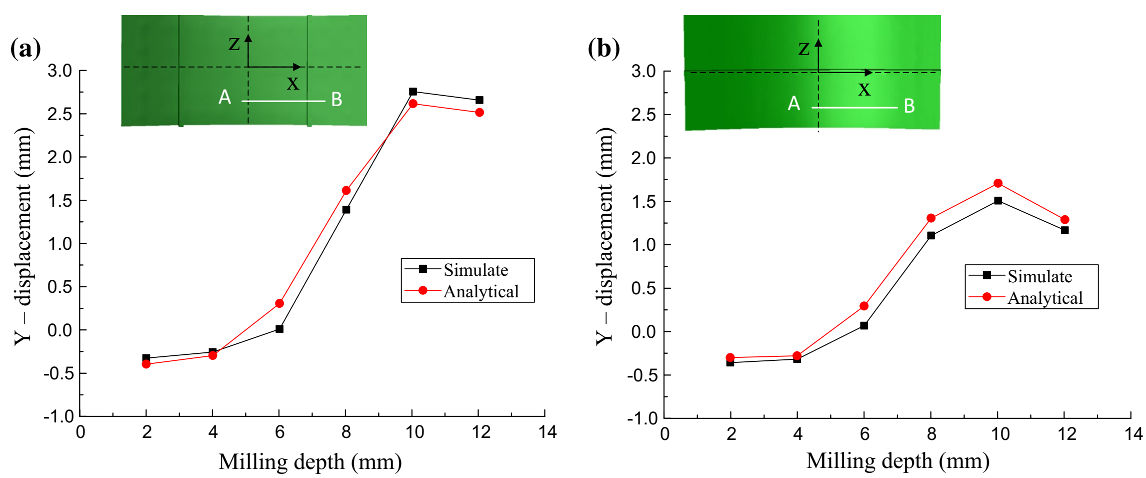

Fig. 9 Springback value of the panel after springback in different cutting depths: **a** crosswise-stiffened panel; **b** lengthwise-stiffened panel

in Fig. 8a, which is mainly caused by the bending residual stress error.

Changes of stress component in x direction in the stiffeners are also presented in Fig. 8. According to Eq. (29), the stress variation in the stiffeners is mainly determined by the radius change. Thus, the stress variation trend is consistent with that in the plate. A maximum stress of 440 MPa occurred at a milling depth of 10 mm, where the plate had maximal springback, and the variation of the stress reached a maximum value of 110 MPa. In Fig. 8a, b, the error distributed more uniformly along the thickness direction, which is mainly caused by initial bending residual stress error. However, when the milling depth increased, the error below the neutral surface decreased and the error above the neutral surface increased. This is because in the milling process, the neutral surface moving to the positive direction of y-axis. The distance between the concave surface and the neutral layer increases, and according to Eq. (27), the stress variation caused by springback is greater. In this situation, some error can be offset. In the contrary, the error above the neutral can hardly decrease.

Compared with two types of stiffened panels, the average standard deviation for crosswise-stiffened panel was 46.3 MPa and for lengthwise-stiffened panel was 38.4 MPa. For the lengthwise-stiffened panel, the increment of errors was smaller because the larger moment of inertia reduced the panel deformation and restrained the errors. In summary, the lengthwise-stiffened panel was less affected by errors than the crosswise-stiffened panel.

4.3 Springback of the Stiffened Panel

Taking the center of the plate as the reference point, we selected the maximum displacement after springback in the y-direction to describe the springback value. Figure 9 shows the maximum springback of two types of stiffened panels when the layers were removed. When the plate was milled between 2 and 4 mm, the displacements were negative. This result is attributed to the stress value of the layer and distance to the neutral surface, which have different signs, so the bending moment is negative, as shown in Fig. 6. According to Eq. (19), the springback is in the convex direction. When the milling depth was 6–10 mm, the total bending moment became positive, and the springback was in the concave direction. At a milling depth of 10 mm, the springback maximized at the original neutral surface. When the plate was milled with 12 mm, the stress became positive again, and the springback value decreased. During the entire milling process, the neutral surface sustained the movement in the convex direction.

The figures also show that the analytical value is consistent with the simulated value. For the crosswise-stiffened panel in Fig. 9a, the maximum positive displacement was 2.74 mm for the FEM and 2.6 mm for the analytical method when the milling depth was 10 mm. In Fig. 9b, the maximum springback value reached a value of 1.5 mm for the FEM and 1.71 mm for the analytical approach. In both pictures, the maximum springback error appeared when the milling depth was 6 mm (0.3 mm for Fig. 9a and 0.23 mm for Fig. 9b). This is because the panel occurs a reverse springback, which enlarges the error. Comparing the two types of panels, the standard deviation of the errors for each panel was 0.175 mm (crosswise) and 0.159 mm (lengthwise) respectively. The springback value and corresponding errors of the lengthwise-stiffened panel are smaller than those of the crosswise-stiffened panel because of the larger moment of inertia.

4.4 Effect of Different Milling Layer Thicknesses

The effect of different milling layer thicknesses was analyzed. The plate was fixed and milled to 12 mm with three milling layer thicknesses of 1, 2, and 3 mm. The springback value results are shown in Fig. 10. The maximum springback value for the crosswise-stiffened panel was approximately 2.64 mm (FEM) when the layer was 2 mm thick, and the relative error was about 10%. The displacements varied when the layer thickness changed to 1 and 3 mm. The difference results from different additional bending moment and force generated per layer, which will affect the stress redistribution in the remaining plate. Therefore, the final total bending moments of three conditions are different as seen from Fig. 10b. In the analytical approach, according to Eqs. (16)–(18), the total bending moment was approximately 103 N m with the layer thickness of 2 mm for the crosswise-stiffened panel. However, the moments were 58 and 50 N m

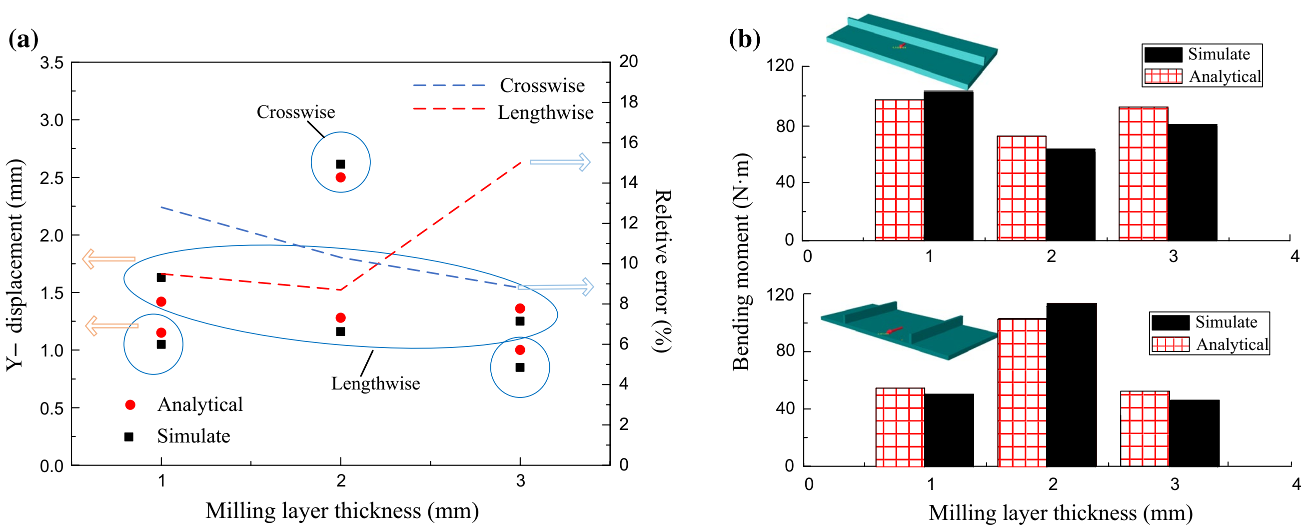

Fig. 10 Springback value with different milling layer thicknesses: **a** crosswise-stiffened panel; **b** lengthwise-stiffened panel

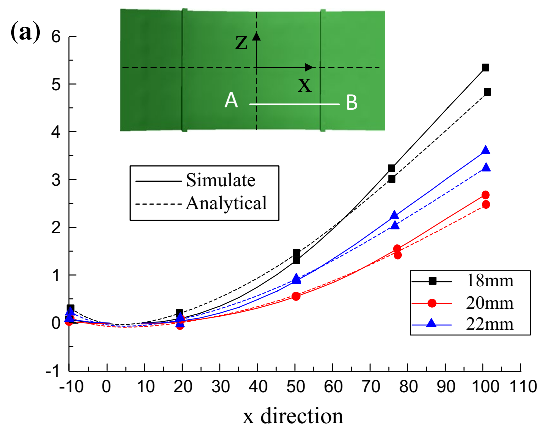

Fig. 11 Springback value with different initial plate thicknesses: **a** crosswise-stiffened panel; **b** lengthwise-stiffened panel

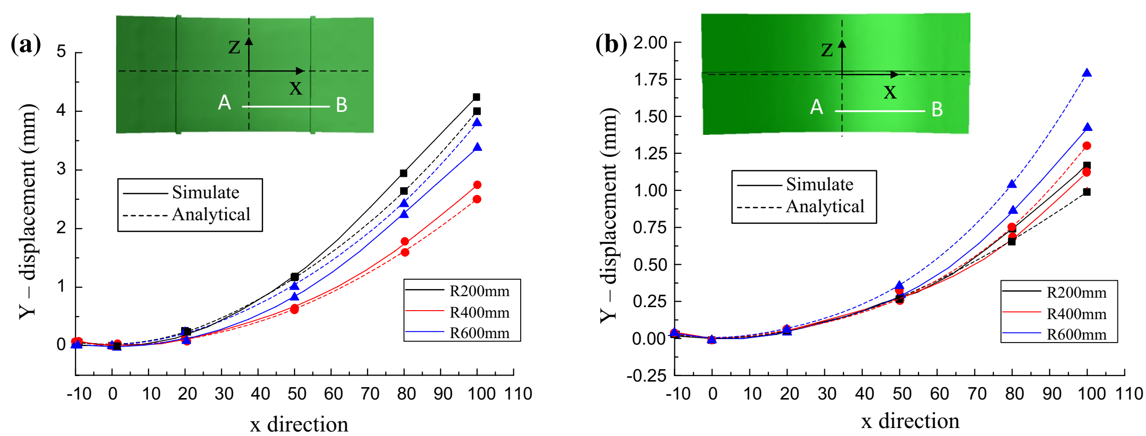

Fig. 12 Springback value with different bending radii: **a** crosswise-stiffened panel; **b** lengthwise-stiffened panel

for the layer thicknesses of 1 and 3 mm, respectively. The errors of bending moment ranges from 4 to 12%.

4.5 Effect of Different Thicknesses and Bending Radii

The milling processes of the plates with different initial plate thicknesses were simulated, where three different plate thicknesses of 18, 20 and 22 mm were designed. The results in Fig. 11 shows that different plate thicknesses remarkably affect the springback. The maximum springback value was 5.35 mm for the crosswise-stiffened panel with a thickness of 18 mm. A thinner plate has a smaller moment of inertia and makes it more liable to springback. However, the 22-mm-thick plate also had larger springback than the 20-mm-thick plate, considering that the milling depth was approximately the neutral surface, which causes a larger bending moment. For the plate with different thicknesses, the springback value is the result of the combined action of the bending moment and moment of inertia. Comparing two methods, the maximum error of the crosswise-stiffened panel was 0.35 mm for a thickness of 18 mm; the other errors were 0.11 and 0.2 mm for thicknesses of 20 and 22 mm. For the lengthwise-stiffened panel in Fig. 8b, the errors were relatively small (0.1–0.3 mm).

Figure 12 presents the comparison of springback because of different bending radii values of 200, 400 and 600 mm. The maximum springback value was 4.2 mm at the bending radius of 200 mm. After springback, the radius variation for R200 mm decreased because the larger plastic strain was contained. However, this plate has a larger curvature, so a notably small change will induce a large springback variation. For a radius of R600 mm, the springback was also larger than that of R400 mm because the plate contains substantial elastic strain, which makes the plate more prone to springback. The maximum error of the two methods for the crosswise panel was 0.5 mm for the radius of R600 mm and 0.2–0.4 mm for the lengthwise panels.

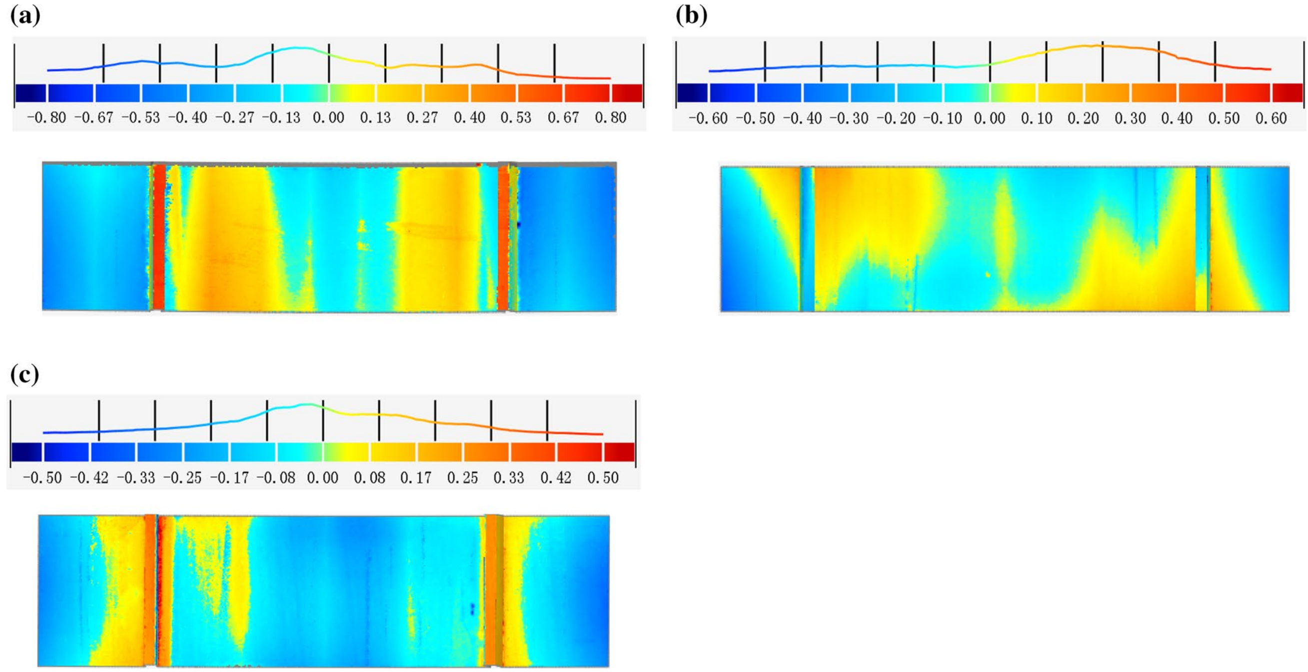

Fig. 13 Comparison of springback between FEM and ANA for crosswise-stiffened panels in different radius radius: **a** R = 200 mm, **b** R = 400 mm and **c** R = 600 mm

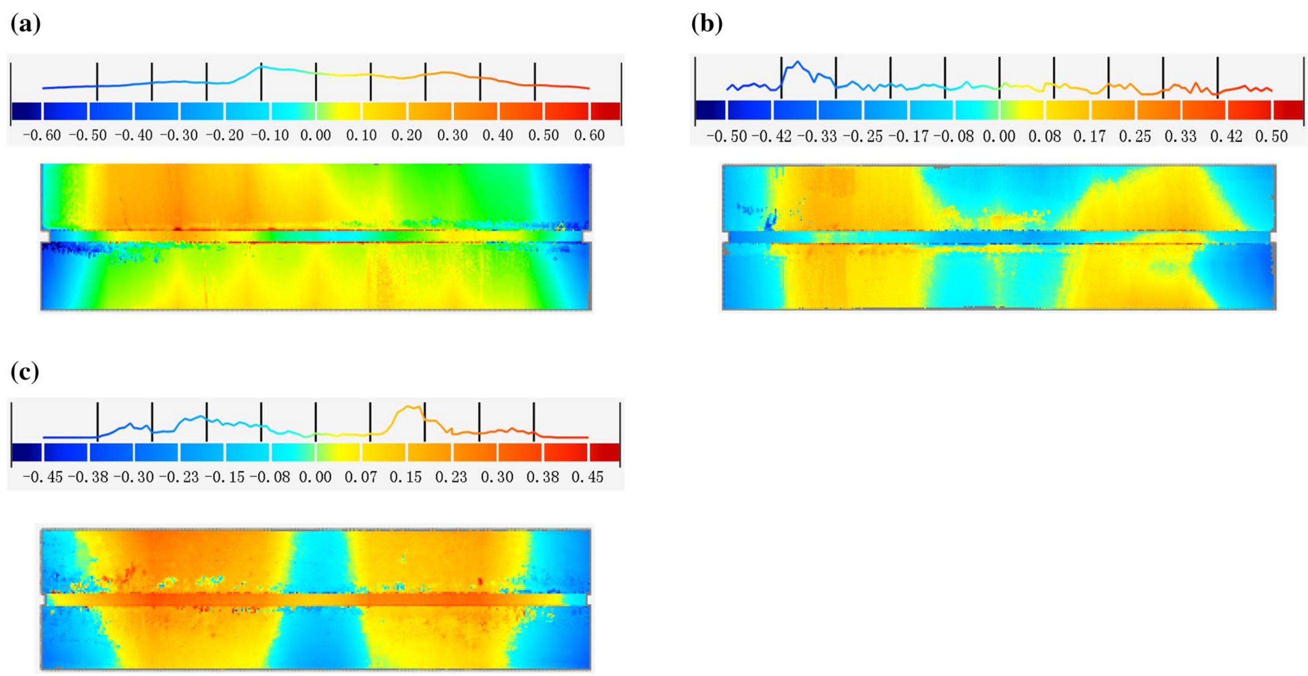

Fig. 14 Comparison of springback between FEM and ANA for lengthwise-stiffened panels in different radius radius: **a** R = 200 mm, **b** R = 400 mm and **c** R = 600 m

Table 4 Maximum displacement and the springback errors compared with experiment

	Lengthwise		Crosswise	
	Maximum displacement (mm)	Percentage errors	Maximum displacement (mm)	Percentage errors
200 mm				
Analytical	1	37.5	4	16.7
FEM	1.25	15.6	4.2	14.3
EXP	1.6	0	4.8	0
400 mm				
Analytical	1.28	15.8	2.5	13.8
FEM	1.16	23.6	2.6	10.3
EXP	1.52	0	2.9	0
600 mm				
Analytical	1.8	18.2	3.8	9.5
FEM	1.5	31.2	3.3	21.4
EXP	2.2	0	4.2	0

4.6 Springback Comparison with the Experiment Results

Figure 13 presents the errors between experimental results and analytical results for crosswise-stiffened panels in different bending radius. From both sides to the center in longitude direction, the errors turn from negative to positive. It means that the radius acquired from analytical method is a little smaller than experiment results. And the errors distribute asymmetrically since the inhomogeneous deformation of the plate. As seen from Fig. 13a, disregarded the errors in stiffeners, the maximum error appears on the right side of the panel, whose value was 0.8 mm. When the bending radius was 400 mm, the maximum error decreased to 0.6 mm and the distribution of the errors was more uniform. When the bending radius was 600 mm, the errors ranged from 0.3 to 0.5 mm. The percentage of the errors ranged from 11 to 17%, which were similar with the FEM results.

Figure 14 shows the springback comparison between analytical results and experimental results for lengthwise-stiffened panels. Seen from Fig. 14a, the maximum error was about 0.6 mm, and in most areas the errors were below 0.3 mm. When the bending radius was 400 mm, the maximum error was further reduced to 0.5 mm. When the radius reached 600 mm, the errors varied from − 0.45 to 0.45 mm. Consistent with the FEM results, the errors of lengthwise-stiffened panels were smaller than that of the crosswise ones. Moreover, compared with the crosswise-stiffened panels, the distribution of the errors is much symmetrical, which means the springback of the lengthwise-stiffened panels were more uniform.

Table 4 indicates the maximum displacements of three approaches in the y-direction for two kinds of panels. To make it more clear, the results of other two methods were compared with the experimental results to acquire the percentage errors. The maximum difference between analytical approach and experiment was 0.8 mm when the bending radius 200 mm for the crosswise-stiffened panels. And for the lengthwise-stiffenend panels, the displacement errors were reletively smaller, whereas the percentage errors were larger. This mainly because the moment of inertia of the panel is larger, leading to a smaller springback value after milling as shown in the table, thus the percentage of error is higher. Moreover, as seen from table, the experimental values were always larger than analytical values and FEM values. The reason is when the plate is bending, the arm of force at both sides of the plate is smaller, which results in the larger elastic strain and less plastic strain. After the bent plate is milled, this area is more liable to spingback.

5 Conclusions

An analytical method to predict the springback of a bending plate after milling into a stiffened panel was proposed. The following conclusions are suggested based on the above findings:

1. The analytical method, which considers the redistribution of residual stress in the remaining plate after milling, has been verified with the FEM and experiment. The analytical results are consistent with the FEM and experimental results, which proves that the method provides an effective approach to predict the springback of the bent plate during the milling process.
2. The analytical and FEM results have identical variation trends of residual stress. The maximum stress variation occurred when the milling depth reached the initial neutral surface of the plate. The method can predict the residual stress distribution in the stiffened panels in certain conditions according to demand.
3. When milling is performed to the initial neutral surface, the bending moment reaches an extreme value with maximum stress variation, whereas the maximum springback value occurs. With the decrease in plate thickness, the springback errors of the two methods increase because the calculation errors accumulate. However, because of the larger moment of inertia, the lengthwise-stiffened

panel have smaller errors than the crosswise-stiffened panel.

The springback prediction method presented in this paper can also be applied to other similar forming conditions. It has certain theoretical guidance meaning for milling process of the bent plate. Through the method, the residual stress and springback involved in milling process can be predicted scientifically.

References

1. Yan, Y. (2009). *Forming modeling and path optimization technology forpress bending of aluminum alloy high-stiffener integral panel* (pp. 60–66). Beijing: School of Mechanical Engineering and Automation, Beihang University.
2. Yan, Y., Wang, H. B., & Wan, M. (2011). Prediction of stiffener buckling in press bend forming of integral panels. *Journal of Plasticity Engineering, 21*(11), 2459–2465.
3. Li, B. Y. (2015). *Research on machining deformation technologies for wallboard on cutting force and residual stress* (pp. 15–16). Harbin: Harbin Institute of Technology.
4. Dong, Y. N. (2016). *Prediction and control of fracture in multipoint press forming of aluminum alloy integral panel* (pp. 8–9). Jilin: Jilin University.
5. Meng, L. H., Atli, M., & He, N. (2017). Measurement of equivalent residual stresses generated by milling and corresponding deformation prediction. *Precision Engineering, 50,* 160–170.
6. Krottenthaler, M., Schmid, C., & Schaufler, J. (2013). A simple method for residual stress measurements in thin films by means of focused ion beam milling and digital image correlation. *Surface & Coatings Technology, 215,* 247–252.
7. Sebastiani, M., Eberl, C., & Bemporad, E. (2014). Focused ion beam four-slot milling for Poisson's ratio and residual stress evaluation at the micron scale. *Surface & Coatings Technology, 251,* 51–61.
8. Vilčeka, I., Řehořa, J., & Caroua, D. (2017). Residual stresses evaluation in precision milling of hardened steel based on the deflection-electrochemical etching technique. *Robotics and Computer-Integrated Manufacturing, 47,* 112–116.
9. Wang, G. Q., Lei, M. K., & Guo, D. M. (2016). Interactions between surface integrity parameters on AISI 304 austenitic stainless steel components by ultrasonic impact treatment. *Procedia CIRP, 45,* 323–326.
10. Lundberg, M., Saarimäki, J., & Moverare, J. (2017). Surface integrity and fatigue behaviour of electric discharged machined and milled austenitic stainless steel. *Materials Characterization, 124,* 215–222.
11. Zhou, N., Peng, R. L., & Pettersson, R. (2016). Surface integrity of 2304 duplex stainless steel after different grindingoperations. *Journal of Materials Processing Technology, 229,* 294–304.
12. Sun, J., & Guo, Y. B. (2009). A comprehensive experimental study on surface integrity by end milling Ti–6Al–4 V. *Journal of Materials Processing Technology, 209*(8), 4036–4042.
13. Arunachalam, R. M., Mannan, M. A., & Spowage, A. C. (2004). Residual stress and surface roughness when facing age hardened Inconel 718 with CBN and ceramic cutting tools. *International Journal of Machine Tools and Manufacture, 44*(9), 879–887.
14. Li, B. Z., Jiang, X. H., & Yang, J. G. (2015). Effects of depth of cut on the redistribution of residual stress and distortion during the milling of thin-walled part. *Journal of Materials Processing Technology, 216,* 223–233.
15. Ma, Y., Feng, P. F., & Zhang, J. F. (2016). Prediction of surface residual stress after end milling based on cutting force and temperature. *Journal of Materials Processing Technology, 235,* 41–48.
16. Liang, S. Y., & Su, J. C. (2007). Residual stress modelling in orthogonal machining. *CIRP Annals-Manufacturing Technology, 56*(1), 65–68.
17. Huang, K., & Yang, W. Y. (2016). Analytical modeling of residual stress formation in workpiece material due to cutting. *International Journal of Mechanical Sciences, 114,* 21–34.
18. Salahshoor, M., & Guo, Y. B. (2014). Finite element simulation and experimental validation of residual stresses in high speed dry milling of biodegradable Mg–Ca Alloys. *Procedia CIRP, 80,* 153–159.
19. Yang, D., Liu, Z. Q., & Ren, X. P. (2016). Hybrid modeling with finite element and statistical methods for residual stress prediction in peripheral milling of titanium alloy Ti–6Al–4V. *International Journal of Mechanical Sciences, 108–109,* 29–38.
20. Jiang, H., Umbrello, D., & Shivpuri, R. (2006). Investigation of cutting conditions and cutting edge preparations for enhanced compressive subsurface residual stress in the hard turning of bearing steel. *Journal of Materials Processing Technology, 171*(2), 180–187.
21. Yu, T. X., & Zhang, L. C. (1992). *Plastic bending theory and its application (chapter 2)* (1st ed.). Beijing: Science Press.

Chun-Guo Liu Professor in the College of Materials Science and Engineering, and Roll Forging Research Institute, JilinUniversity. The main interests of his research include Roll forging process design, Intelligent Manufacturing Systems, Complex Systems Modeling, Multi-point forming process design.

Tao Yue Ph.D. in the College of Materials Science and Engineering, and Roll Forging Research Institute, JilinUniversity. The main interests of his research include the manufacturing process of the integral panels, the Mechanics analysis, the Multi-point forming process design.

Xiao-Tong Yu Master in the College of Materials Science and Engineering, and Roll Forging Research Institute, JilinUniversity. The main interests of her research include the release of the residual stress in milling process.